Chemical Science

ROYAL SOCIETY OF CHEMISTRY

EDGE ARTICLE

View Article Online
View Journal | View Issue



Cite this: *Chem. Sci.*, 2025, **16**, 9739

All publication charges for this article have been paid for by the Royal Society of Chemistry

# Electron rearrangement at the crystalline–amorphous heterogeneous interface boosts alkaline hydrogen production†

Meihuan Liu,‡[a] Yuke Gu,‡[a] Hui Su, *[b] Xuanzhi Liu,[a] Juan Luo,[a] Pengfei Tan,*[a] Feng Liu[c] and Jun Pan *[ac]

Received 25th March 2025
Accepted 26th April 2025

DOI: 10.1039/d5sc02271a

rsc.li/chemical-science

Modifying the platinum (Pt) local reaction microenvironment is a critical and complex challenge in enhancing electrochemical performance. Herein, amorphous $Co(OH)_2$ and crystalline Pt (labeled as ac-Pt@$Co(OH)_2$) featuring abundant crystalline–amorphous (c–a) interfaces are designed to boost the hydrogen evolution reaction (HER). The engineered structure creates an advantageous chemical environment at the local level, enhancing hydrogen adsorption efficiency and resulting in exceptional HER performance. The ac-Pt@$Co(OH)_2$ achieves a low Tafel slope of 28.5 mV $dec^{-1}$ and requires merely 95 mV overpotential to reach 200 mA $cm^{-2}$ in alkaline electrolyte (1 M KOH), surpassing those of conventional Pt/C catalysts (39.4 mV $dec^{-1}$, 256 mV). *In situ* advanced characterization investigations reveal dynamic electron rearrangement at the c–a interface, where Co species initially accept electrons from Pt to optimize the adsorption of *H species and then donate electrons to Pt for accelerating reduction kinetics. Theoretical calculations reveal that amorphous $Co(OH)_2$ promotes the dissociation of water molecules to produce active *H, and electron rearrangement at the c–a interface downshifts the d-band center, thereby optimizing the *H adsorption strength and enhancing HER activity. The ac-Pt@$Co(OH)_2$-based alkaline anion-exchange membrane water electrolyzer (AEMWE) maintains a current density of 500 mA $cm^{-2}$ over 500 h.



## 1 Introduction

The extensive depletion of nonrenewable energy sources has triggered significant energy shortages and environmental degradation. In this context, hydrogen ($H_2$) as a clean and renewable energy carrier, has garnered substantial interest.[1,2] Electrochemical water splitting, powered by renewable energy, presents a promising approach for sustainable hydrogen production, although it involves intricate surface reactions. As a half-reaction of alkaline water electrolysis (AWE), the alkaline hydrogen evolution reaction (HER) suffers from sluggish kinetics, being orders of magnitude slower than in acidic electrolytes.[3,4] Thus, developing highly efficient electrocatalysts for alkaline HER, offering both high activity and long-term stability, is crucial for enabling anion exchange membrane water electrolysis (AEMWE). Despite the great success that has been achieved with earth-abundant electrocatalysts including transition-metal sulfides and nitrides for alkaline HER,[5] platinum-based (Pt-based) electrocatalysts are still considered the best choice to catalyze the HER owing to their ideal hydrogen adsorption energy among all pure metals. However, Pt's limited water dissociation ability in alkaline media hinders the generation of protons during the Volmer step, particularly when the hydrogen intermediate strongly adsorbs on the Pt surface. This issue creates significant barriers to enhancing the economic viability of hydrogen production.[6–9] Consequently, a reasonable design of catalysts for alkaline HER requires simultaneously promoting the capabilities of water adsorption and dissociation on catalysts and precisely regulating the electronic structure of metal sites to obtain appropriate Pt–H interactions; this remains a highly sought-after goal and a substantial challenge.

Significant research focus has been directed toward optimizing platinum catalytic centers for improved HER kinetics through metal alloying,[10,11] morphology tuning,[12] and interface engineering.[13] Among the available catalyst design and synthesis strategies, constructing heterostructures *via* interface engineering stands out due to its distinct advantages for energy storage and conversion. These heterostructures, comprising different materials, can leverage the strengths of each component while mitigating their respective weaknesses.[14] The

[a]*State Key Laboratory for Powder Metallurgy, Central South University, Changsha 410083, Hunan, China. E-mail: tpf0203@csu.edu.cn; jun.pan@csu.edu.cn*

[b]*Key Laboratory of Light Energy Conversion Materials of Hunan Province College, College of Chemistry and Chemical Engineering, Hunan Normal University, Changsha 410081, Hunan, China. E-mail: suhui@hunnu.edu.cn*

[c]*Yunnan Precious Metals Lab Co., Ltd, Kunming, Yunnan 650106, China*

† Electronic supplementary information (ESI) available. See DOI: https://doi.org/10.1039/d5sc02271a

‡ These authors contributed equally.

formation of an interfacial electric field occurs spontaneously when dissimilar materials possessing distinct work functions come into contact. This phenomenon induces charge redistribution at the atomic scale, facilitating improved electron mobility and strengthening molecular adsorption at active sites, thereby significantly enhancing catalytic activity. Many reports on heterojunction catalysts focus on crystalline–crystalline (c–c) complexes, which may result in a limited number of active sites and lower surface energy.[15,16] In contrast, crystalline–amorphous (c–a) heterostructures have emerged as an auspicious design for electrocatalysis, harnessing the combined advantages of amorphous and crystalline structures and exhibiting unconventional atomic arrangements at the heterostructure interface.[17–20] Specifically, Pt is insufficient for the water dissociation step in alkaline media, it is typically difficult to break the scaling relationship of key intermediates in the alkaline HER with a single catalytic site.[21–23] Hence further improving the activity and stability of the Pt-based HER catalyst remains a hot research topic. Pt-based materials integrated with transition hydroxides generally show superior hydrophilicity and optimal binding of *OH, which helps prevent catalyst deactivation during the HER.[24,25] Enlightened by this guideline, designing a heterogeneous transition hydroxide-decorated Pt catalyst with abundant c–a interfaces is a viable method to regulate water dissociation barriers and hydrogen adsorption energy, ultimately improving both activity and stability for the alkaline HER.

Here, we construct a c–a heterogeneous catalyst composed of amorphous $Co(OH)_2$ and crystalline Pt (labeled as ac-Pt@$Co(OH)_2$) with enhanced water-dissociation ability for highly active and stable alkaline HER catalysis in AEMWEs. As a proof-of-concept, the introduction of the c–a interface and $Co(OH)_2$ in ac-Pt@$Co(OH)_2$ not only induces interfacial charge redistribution but also facilitates the dissociation of water, ensuring an abundant proton supply to the catalyst and significantly altering the HER kinetics. As a result, ac-Pt@$Co(OH)_2$ exhibits superb HER activity (35 mV@10 mA $cm^{-2}$) with an acid-like Tafel slope of 28.5 mV $dec^{-1}$. *In situ* characterization validate that the c–a interfaces play vital roles in activating the alkaline HER. Concretely, the generation of Pt–*H can be directly observed by *in situ* Raman spectroscopy, indicating enhanced water dissociation. *In situ* X-ray absorption fine structure (XAFS) spectroscopy reveals the dynamic electron rearrangement at the c–a interface, in which Co species initially accept electrons from Pt to optimize the adsorption of *H species and later donate electrons back to Pt, accelerating the reduction kinetics. This suggests that the local coordination environment of Pt is altered by $Co(OH)_2$. Notably, the ac-Pt@$Co(OH)_2$-based AEMWE operating with 1 M KOH requires only 1.76 V to reach a high current density of 0.5 A $cm^{-2}$, showing a negligible voltage increase for 500 h. This research offers a comprehensive investigation of the active components and reaction mechanisms involved in crystalline–amorphous heterostructures, highlighting the great potential of c–a heterostructure catalyst design for advanced energy technologies.

# 2 Results and discussion

## 2.1 Material synthesis and characterization

The ac-Pt@$Co(OH)_2$ catalyst with crystalline–amorphous boundaries was synthesized *via* a "template-solvent" strategy. Initially, Pt and Co species were absorbed into the mesoporous KIT-6 template. Then, the mixed solution, after adding a reducing agent, was treated with hot NaOH, simultaneously removing the template and producing amorphous $Co(OH)_2$ decorated on crystalline Pt. The powder X-ray diffraction (XRD) studies show a face-centered cubic Pt crystalline structure for c-Pt (PDF#04-0802). The obtained ac-Pt@$Co(OH)_2$ sample has a similar crystalline structure as c-Pt (Fig. 1a), with characteristic peaks attributed to the (111), (200), (220), and (311) planes of cubic Pt.[23,26] However, no obvious diffraction peak related to Co species can be found, suggesting an amorphous nature of Co-containing species in ac-Pt@$Co(OH)_2$. To clarify the composition, the materials were further characterized by Raman spectrometry. As shown in Fig. 1b, the peak that appeared at approximately 500 $cm^{-1}$ in ac-Pt@$Co(OH)_2$ can be assigned to cobalt hydroxide,[27] indicating the formation of amorphous $Co(OH)_2$ in the hybrid ac-Pt@$Co(OH)_2$ material. Moreover, the $k^3\chi$ ($k$) oscillation curve for the Co K-edge in ac-Pt@$Co(OH)_2$ (Fig. S1†) is different from those of Co and CoO, while closely resembling that of $Co(OH)_2$. The above results verify that Co is mainly in the form of amorphous $Co(OH)_2$ in ac-Pt@$Co(OH)_2$. Analysis of the Fourier transform extended X-ray absorption fine structure (EXAFS) signal of ac-Pt@$Co(OH)_2$ reveals distinct coordination features in Fig. 1c. The primary coordination shell, corresponding to Co–O bonds, appears at 1.59 Å, while the secondary coordination sphere, representing Co–Co interactions, is observed at 2.69 Å. Notably, the peak intensity associated with Co–Co coordination shows significant attenuation compared to standard $Co(OH)_2$. This reduction in signal strength indicates substantial structural disordering within the amorphous $Co(OH)_2$ nanosheets.[28]

The transmission electron microscopy image (TEM) (Fig. 1d) exhibits that ac-Pt@$Co(OH)_2$ has a meso-channel-penetrated polyhedral morphology. At the same time, the ac-Pt@$Co(OH)_2$ sample is constructed with nanoparticles embedded in the nanosheet. As shown in Fig. 1e and S2,† energy-dispersive X-ray spectroscopy (EDX) mapping confirms the existence of Pt, Co, and O, and the Co-containing nanosheet across the ac-Pt@$Co(OH)_2$ sample. Moreover, the magnified high-resolution TEM (HRTEM) image in Fig. 1f displays that ac-Pt@$Co(OH)_2$ is composed of amorphous $Co(OH)_2$ (yellow region) and crystalline domains. Meanwhile, the Pt sample shows a similar morphology (Fig. S3†). The selected-area fast Fourier transform (FFT) pattern and the corresponding inverse fast Fourier transform (IFFT) image (Fig. 1g) from the crystalline domain display a lattice fringe spacing of 0.220 nm, which can be attributed to the (111) plane of Pt. By contrast, the FFT analysis in area 2 (Fig. 1h) displays typical features of an amorphous structure. Furthermore, the FFT pattern (area 3) has verified the amorphous–crystalline boundary with the coexistence of diffuse-rings and diffraction spots (Fig. 1i). Meanwhile, the

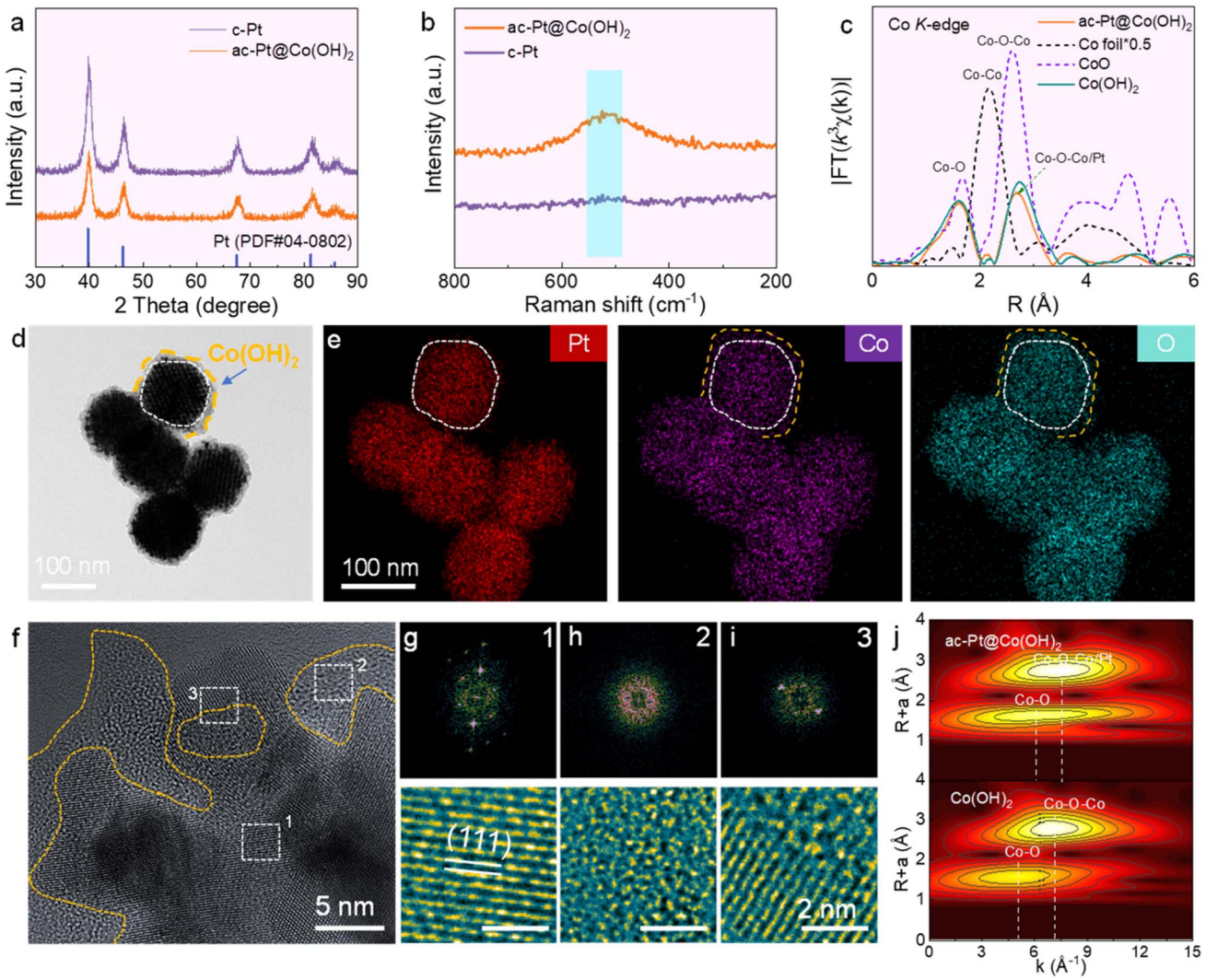


Fig. 1 (a) XRD patterns and (b) Raman patterns of c-Pt and ac-Pt@$Co(OH)_2$. (c) EXAFS spectra at the Co K-edge. (d) TEM, (e) EDX element mappings, and (f) HRTEM images of ac-Pt@$Co(OH)_2$. (g–i) FFT and corresponding IFFT patterns of the selected regions in (f). (j) WT for the Co $k^3$-weighted EXAFS signal of $Co(OH)_2$ and ac-Pt@$Co(OH)_2$.

wavelet transform (WT) analysis of the EXAFS data reveals significant changes in the *k*-space characteristics of Co–Co coordination. Compared to the reference $Co(OH)_2$ sample, which displays a characteristic signal at 7.1 $Å^{-1}$, the ac-Pt@$Co(OH)_2$ composites exhibit a distinct shift to higher *k*-space values (7.6 $Å^{-1}$) (Fig. 1j). This observed displacement in the wavelet transform maximum indicates potential coordination interactions between cobalt and platinum atoms within the composite structure.[28]

To elucidate the local electronic and coordination structural information of ac-Pt@$Co(OH)_2$, X-ray photoelectron spectroscopy (XPS) and X-ray absorption fine structure (XAFS) measurements were employed. As shown in Fig. 2a, the high-resolution Co 2p signal of ac-Pt@$Co(OH)_2$ can be deconvoluted into two peaks of 780.8 and 796.9 eV, with two shake-up satellite peaks, which are mainly characteristic features of $Co^{2+}$ from $Co(OH)_2$ on the surface.[29] Furthermore, the O 1s region spectrum (Fig. 2b) exhibits two oxygen contributions. The main O 1s peak at 530.9 eV is usually consistent with oxygen in $OH^-$ groups.[30] The peaks at 532.2 eV represent the presence of chemisorbed structural water on the surface.[31] In addition, Fig. 2c depicts the coexistence of both metallic and oxidized platinum species in the ac-Pt@$Co(OH)_2$ composite, with the metallic form being predominant. The binding energy positions corresponding to metallic Pt $4f_{7/2}$ and Pt $4f_{5/2}$ orbitals are observed at 71.4 eV and 74.7 eV, respectively. These values demonstrate a positive energy shift relative to Pt, indicating electronic structure modification of the Pt sites in ac-Pt@$Co(OH)_2$ due to the electron redistribution at the c–a heterogeneous interface.[32] Note that the XAFS signal is an average of all the targeted atoms. Compared with Co foil and $Co(OH)_2$, the Co absorption edge in ac-Pt@$Co(OH)_2$ (Fig. 2d) is slightly more negative than standard $Co(OH)_2$, which may be attributed to electron donation from Pt.[33] Furthermore, the white line peak intensity of the Pt $L_3$ edge (Fig. 2e and S4†) demonstrates an elevated Pt valence in the heterostructure compared to Pt,[34] corroborating the XPS results on electron transfer. This indicates increased charge transfer from Pt to Co

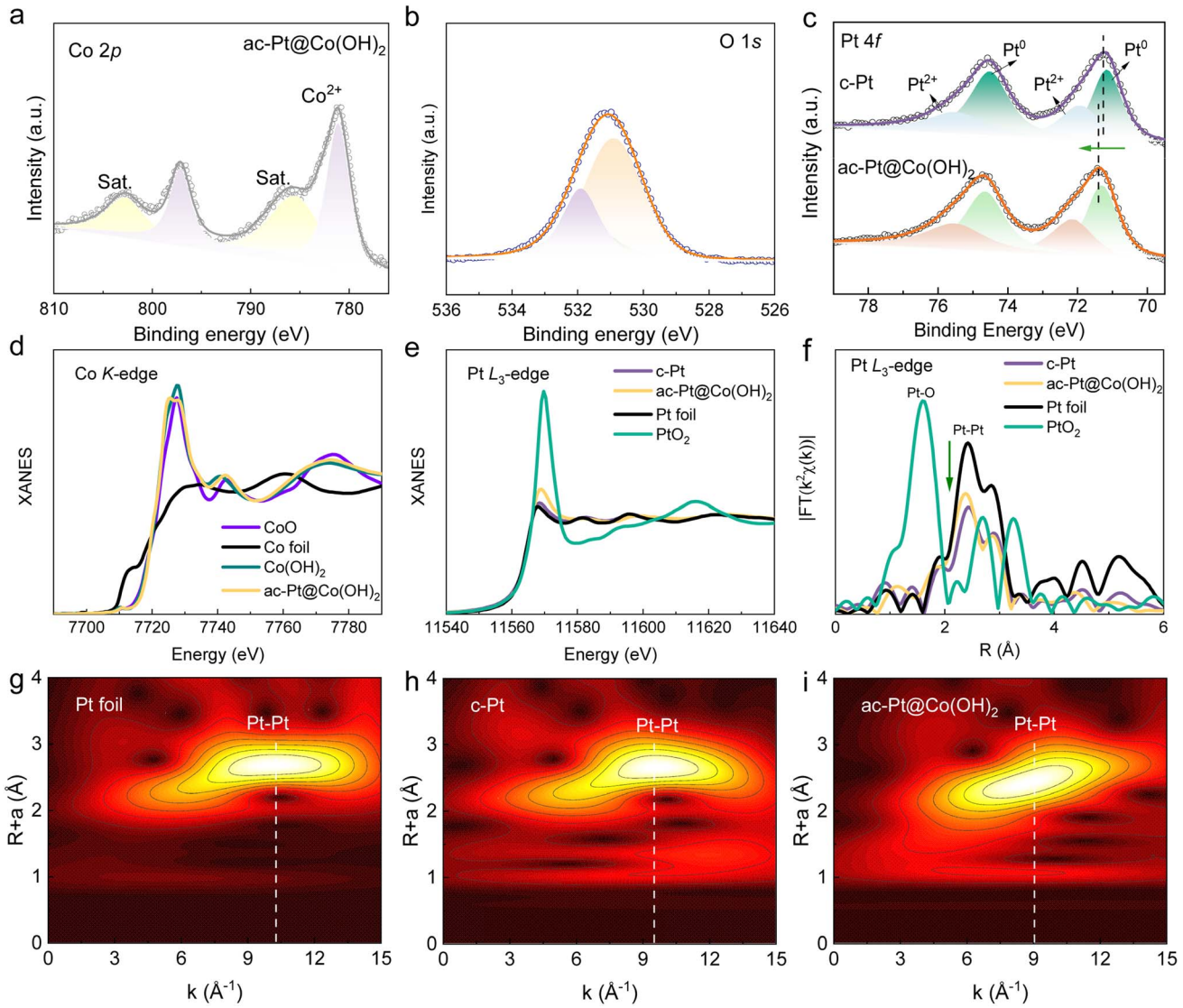


Fig. 2 (a) Co 2p and (b) O 1s XPS spectra of ac-Pt@Co(OH)$_2$. (c) Pt 4f XPS spectra of ac-Pt@Co(OH)$_2$ and c-Pt. (d and e) Co K-edge and Pt $L_3$-edge XANES spectra. (f) EXAFS spectra at the Pt $L_3$-edge. (g–i) WT-EXAFS plots of the Pt $L_3$-edge for Pt foil, c-Pt, and ac-Pt@Co(OH)$_2$.

due to the construction of the c–a interface between Pt and Co(OH)$_2$. Moreover, the EXAFS spectrum of ac-Pt@Co(OH)$_2$ (Fig. 2f) shows a dominant peak at 2.42 Å that is shorter than that of c-Pt, suggesting the existence of the Pt–Pt/Co bond. Furthermore, the peak intensity of ac-Pt@Co(OH)$_2$ and c-Pt is also significantly lower than that of Pt foil, which means that the catalyst prepared by the KIT-6 template method leads to a large number of porous structures, resulting in a decrease in the coordination number. Meanwhile, the WT-EXAFS spectra in Fig. 2g–i show that ac-Pt@Co(OH)$_2$ exhibits a maximum intensity value for Pt–Pt/Co at ~9.0 Å in $k$ space, which is smaller than the ~9.5 Å observed for Pt, further revealing that Pt is coordinated with a lighter Co element.[35]

### 2.2 Electrocatalytic HER performance

The electrochemical performance of ac-Pt@Co(OH)$_2$ toward the HER was evaluated in 1 M KOH electrolyte. For comparison, Pt and commercial Pt/C (20%) catalysts were also assessed (Fig. 3a). All potentials stated here are relative to the reversible hydrogen electrode (*versus* RHE). As presented in Fig. 3b, the as-prepared ac-Pt@Co(OH)$_2$ requires ultralow overpotentials of 35 and 95 mV to deliver the current densities of 10 and 200 mA cm$^{-2}$, respectively, superior to c-Pt ($\eta_{10} = 66$ mV; $\eta_{200} = 204$ mV) and Pt/C ($\eta_{10} = 51$ mV; $\eta_{200} = 256$ mV). The corresponding Tafel plots were achieved to illuminate the underlying reaction kinetics (Fig. 3c). The ac-Pt@Co(OH)$_2$ possesses a Tafel slope of 28.5 mV dec$^{-1}$, smaller than those of Pt and Pt/C. This implies faster reaction kinetics in the alkaline HER process. The ac-Pt@Co(OH)$_2$ demonstrates a lower charge transfer resistance compared to c-Pt and Pt/C catalysts (Fig. S5†), suggesting that ac-Pt@Co(OH)$_2$ may exhibit improved HER activities. Remarkably, ac-Pt@Co(OH)$_2$ achieves a mass activity of 1.64 A $mg_{Pt}^{-1}$ (Fig. 3d) at an overpotential of 50 mV, which is 7.5 and 4.2 times higher than that of c-Pt and Pt/C, respectively. Combining the

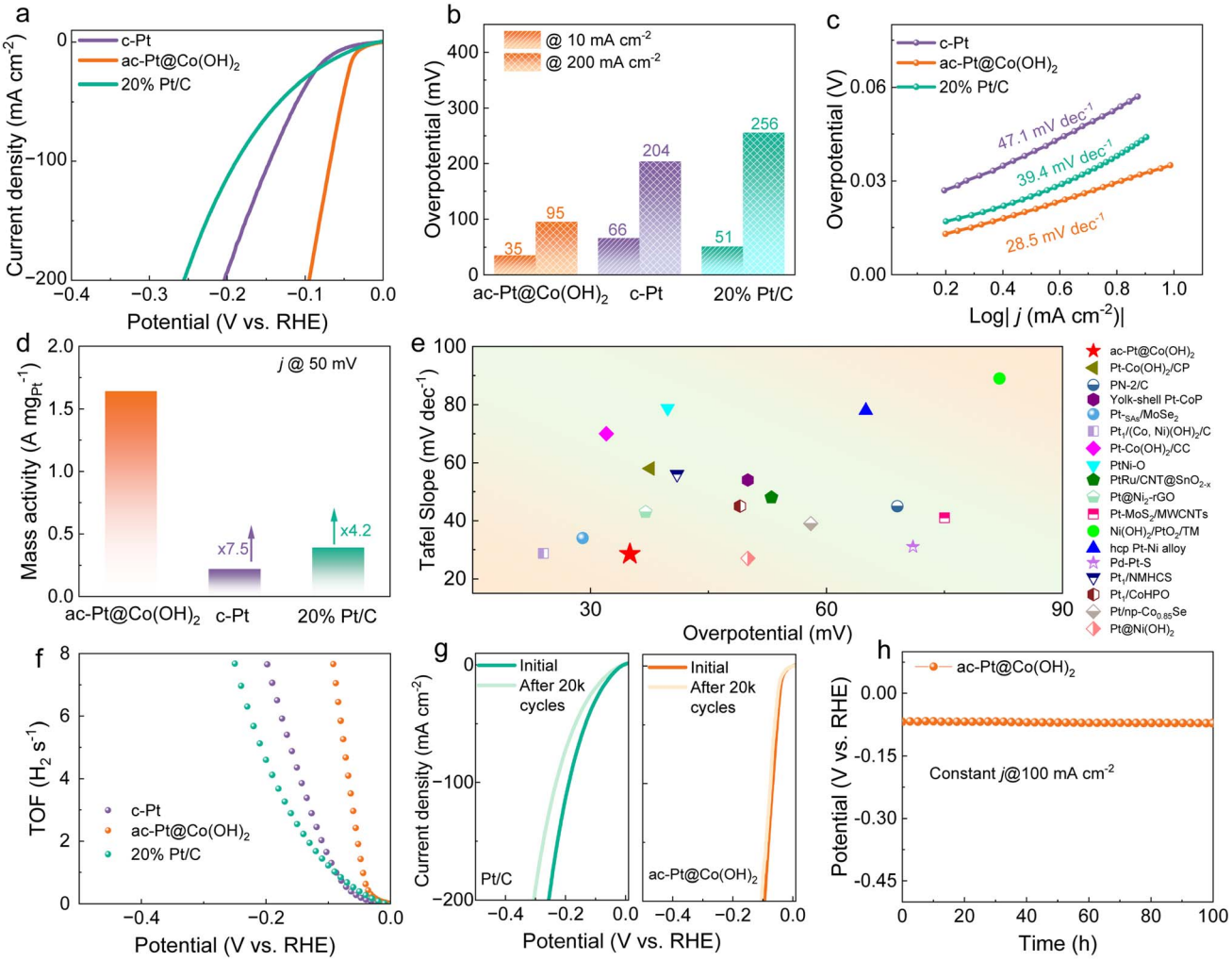


Fig. 3 (a) Polarization curves of the electrocatalysts. (b) Comparison of $\eta_{10}$ and $\eta_{200}$ for the electrocatalysts. (c) Tafel plots to assess the kinetics of the electrocatalytic reactions. (d) Mass activity at an overpotential of 50 mV (*vs.* RHE). (e) Comparison of overpotential at 10 mA cm$^{-2}$ and Tafel slopes for ac-Pt@Co(OH)$_2$ and recently reported HER catalysts.[13,23,28,36–49] (f) TOF values of ac-Pt@Co(OH)$_2$, c-Pt, and Pt/C catalysts. (g) Polarization curves of ac-Pt@Co(OH)$_2$ and Pt/C before and after 20 000 cycles. (h) Chronopotentiometric measurements of ac-Pt@Co(OH)$_2$; carbon paper was used as the catalyst support.

Tafel slope and overpotential data, the performance of the prepared ac-Pt@Co(OH)$_2$ is well-placed among certain recent state-of-art Pt-based electrocatalysts (Fig. 3e). To quantify the intrinsic catalytic performance, turnover frequency (TOF) values (Fig. 3f) were systematically calculated and compared. At an overpotential of 50 mV, the ac-Pt@Co(OH)$_2$ exhibits a high TOF of 1.65 s$^{-1}$, outperforming the other two catalysts. Beyond activity assessment, the material's stability was thoroughly investigated through comprehensive electrochemical testing protocols, including accelerated stress tests and chronopotentiometric analysis. As depicted in Fig. 3g, the polarization curves of ac-Pt@Co(OH)$_2$ before and after 20 000 cycles almost overlap, whereas the Pt/C catalyst displays significant deterioration in activity. Additionally, negligible potential decay can be observed at a cathodic current density of 100 mA cm$^{-2}$ for ac-Pt@Co(OH)$_2$ during a 100-h chronopotentiometry test. Impressively, the c–a heterogeneous interface of ac-Pt@Co(OH)$_2$ (Fig. S6†) after cycles remains, and the oxidation state of Pt and Co is almost preserved (Fig. S7†). It is convincing to validate that the c–a heterogeneous construction has substantially improved the HER performance.

### 2.3 *In situ* characterization and DFT

To reveal the underlying mechanism of the c–a heterostructure for enhanced HER activity, *in situ* XAFS measurements using a purpose-built cell were conducted on the ac-Pt@Co(OH)$_2$ catalyst during the HER (Fig. S8†). From the *ex situ* conditions (electrodes are immersed in the solution without applying potentials) to the conditions under −0.01 V *versus* RHE (all voltages mentioned hereafter are normalized to the RHE scale), the white-line peak intensity of Pt (Fig. 4a) increases slightly, which may be ascribed to the adsorption of reaction intermediates.[50] With the cathodic potential decreasing to −0.05 V, the Pt white-line peak intensity decays, indicating a reduction of its oxidation state under HER conditions. Additionally, the FT-EXAFS spectra of Pt (Fig. S9†) at different potentials show an

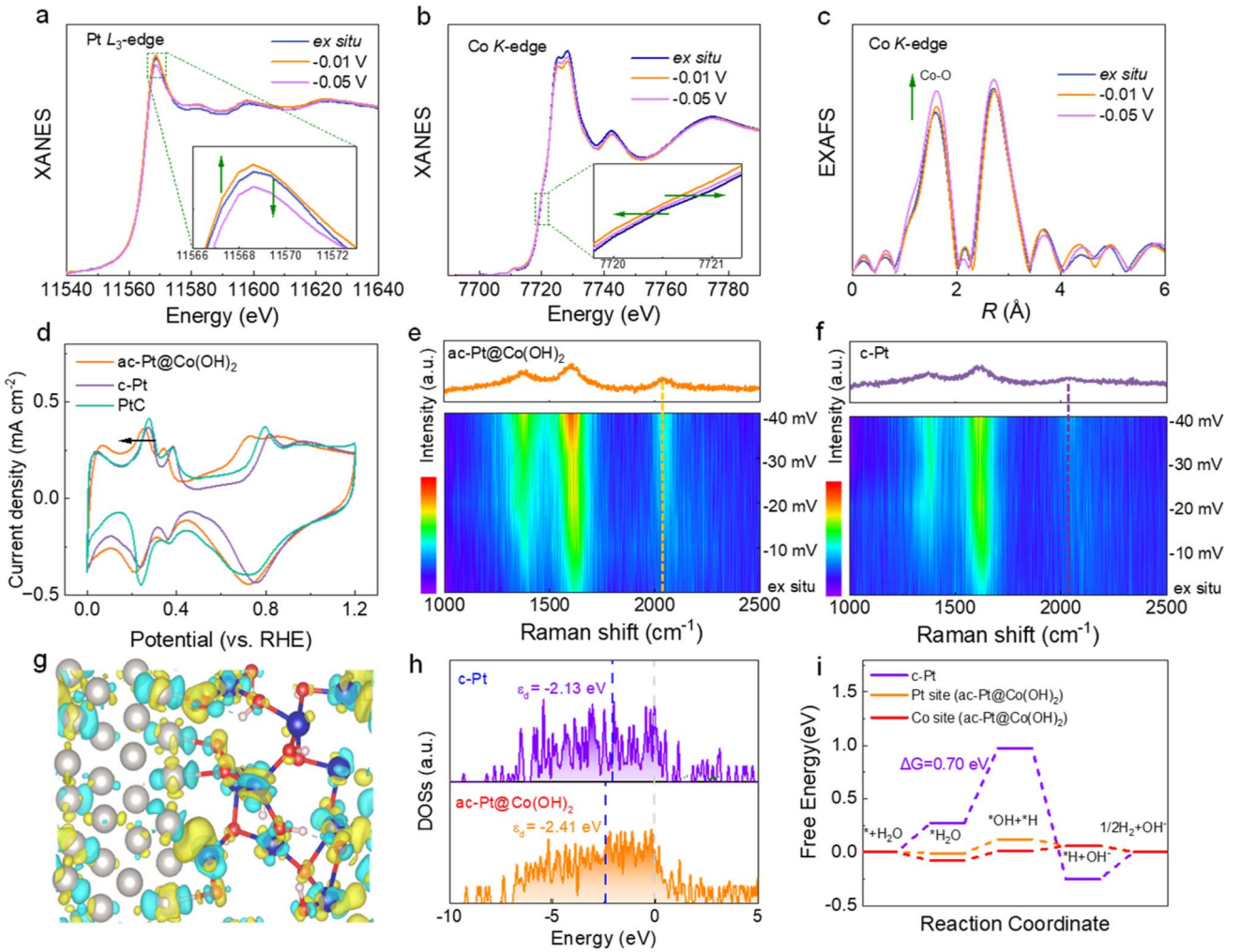


Fig. 4 (a and b) *In situ* XANES spectra for the (a) Pt L-edge, and (b) Co K-edge for ac-Pt@Co(OH)$_2$. (c) *In situ* EXAFS spectra of the Co K-edge. (d) CV curves of ac-Pt@Co(OH)$_2$, c-Pt, and Pt/C. (e and f) *In situ* Raman spectra of (e) ac-Pt@Co(OH)$_2$ and (f) c-Pt. (g) Differential charge density of ac-Pt@Co(OH)$_2$; the yellow color represents the charge accumulation, and the cyan color represents the charge depletion. (h) Density of states (DOS) and (i) free energy change of ac-Pt@Co(OH)$_2$ and c-Pt.

inconspicuous change in the strong peak at 2.42 Å, confirming the desirable structural stability of ac-Pt@Co(OH)$_2$, which can be attributed to the strong interaction between amorphous Co(OH)$_2$ and the crystalline Pt structure.[51] To accurately capture the c–a heterostructure electronic interaction between Co(OH)$_2$ and Pt, Co K-edge XAFS was also conducted to study the dynamic electron interaction behavior during the reaction process. Interestingly, for Co K-edge XANES (Fig. 4b), the position of the absorption edge moves first to the lower energy and then to the higher energy from *ex situ* to −0.1 V and −0.5 V conditions. This suggests that the oxidation state of Co sites changes in the opposite direction compared to Pt, indicating the obvious dynamic electron rearrangement at the c–a heterogeneous interface of ac-Pt@Co(OH)$_2$. Specifically, the Co species act as an electron acceptor to achieve rapid electron transfer from Pt to Co at a small overpotential, suggesting that Co species can regulate the electron state of Pt to optimize the adsorption of *H. Interestingly, at a high overpotential, the Co species can donate electrons back to Pt sites, promoting the reduction reaction kinetics. Furthermore, the FT-EXAFS spectra of Co at different potentials (Fig. 4c) show that as the potential decreases, the intensity of the peak corresponding to the Co–O bonds at ≈1.6 Å gradually increases. This significant enhancement (>3% change) in the intensity of the Co–O peaks with varying voltage can be attributed to adsorbed and dissociated water molecules over Co sites.[52,53]

To probe the hydrogen adsorption characteristics under operational conditions, cyclic voltammetry measurements were conducted across various catalyst samples. This electrochemical approach enables the simulation of hydrogen intermediate (*H) conversion processes that occur during the hydrogen evolution reaction (Fig. 4d). The ac-Pt@Co(OH)$_2$ catalyst negatively shifts the desorption peak potential indicating more intense dissociated *H desorption compared with the reference c-Pt,[54,55] contributing to HER performance improvement. To explore the structural advantages of the ac-Pt@Co(OH)$_2$ catalyst for alkaline HER and the possible reaction mechanisms, the adsorbed species of the catalysts during the

catalytic reaction were detected by *in situ* Raman spectroscopy with c-Pt as a reference. As shown in Fig. 4e and f, the characteristic D and G bands appearing at ~1350 and ~1580 $cm^{-1}$ are derived from the carbon cloth electrode. Meanwhile, a peak at ~2050 $cm^{-1}$ can be assigned to Pt–*H emerging for ac-Pt@Co(OH)$_2$.[56,57] The peak signals intensified under controlled applied potentials (*ex situ* to −0.04 V) compared with that of c-Pt. It suggests that a large amount of active H accumulates at the Pt site, thanks to the strong hydrolytic dissociation capacity of Co(OH)$_2$ to provide a rich active H species. Above all, the *in situ* XAFS and Raman results jointly reveal the obvious electron transfer behavior between Pt and Co sites, and the synergistic effect of the a–c interface accelerates the formation of *H on the catalyst surface, contributing to enhanced HER activity and stability.

Moreover, to understand the synergy between the c–a interface, density functional theory (DFT) calculations were conducted on the charge-density distribution of the catalyst surface and the crucial reaction steps of HER. Theoretical models for c-Pt and heterojunction ac-Pt@Co(OH)$_2$ were used (Fig. S10 and S11†). The difference charge density of ac-Pt@Co(OH)$_2$ demonstrates the charge transfer from Pt to Co through bridged oxygen atoms at the c–a heterogeneous interface (Fig. 4g).[58] This is in good agreement with the XANES results. These results illustrate that the reinforced c–a interfacial interaction could produce electron-deficient Pt sites by redistribution of electrons, which is expected to modify the d-band structure and adsorption properties. As shown in Fig. 4h, the downshift of the d-band center in ac-Pt@Co(OH)$_2$ compared with that of c-Pt, revealing that ac-Pt@Co(OH)$_2$ has an optimal *H desorption ability during the HER process. To investigate the HER activity for the two catalysts, the calculated free energy was presented in Fig. 4i. In addition, for ac-Pt@Co(OH)$_2$, the adsorption of water molecules at Pt and Co sites was considered to clarify the influence of Co(OH)$_2$ and interfacial electron interaction (Fig. S12 and S13†). The rate-determining steps (RDS) on c-Pt and ac-Pt@Co(OH)$_2$ are the $H_2O$ decomposition with a free energy of 0.70 eV, 0.13 eV (Pt site) and 0.09 eV (Co site), respectively, indicating high $H_2O$ splitting capability over amorphous Co(OH)$_2$ in ac-Pt@Co(OH)$_2$.[59] Furthermore, upon introducing Co(OH)$_2$, the adsorption/desorption capability is greatly optimized by the obvious dynamic electron rearrangement effect at the c–a heterogeneous interface. This implies that Pt and Co are synergistic active sites, in which the Co(OH)$_2$ could facilitate water dissociation and ensure efficient proton supply to the active Pt sites under an alkaline electrolyte, resulting in enhanced HER kinetics.

### 2.4 AEMWE performance

Encouraged by its superior HER activity and stability, we assembled a membrane-electrode-assembly (MEA)-based real AEMWE device using iridium-plated titanium felt as the anodic catalyst (Fig. 5a). The prepared catalysts were operated in 1 M KOH electrolyte. Under the same testing conditions, the activity trend of ac-Pt@Co(OH)$_2$ > Pt/C was observed again in the electrolyzers (Fig. 5b). Particularly, a cell voltage of only 1.76 V is needed for ac-Pt@Co(OH)$_2$ to reach a current density of 0.5 A $cm^{-2}$, much lower than that of Pt/C-based AEMWEs. More importantly, the ac-Pt@Co(OH)$_2$ electrolyzer exhibits good long-term stability under 500 mA $cm^{-2}$ with a low attenuation of 0.14 mV $h^{-1}$ (Fig. 5c). All these observations demonstrate that the ac-Pt@Co(OH)$_2$ electrode has excellent activity and exceptional long-term durability, holding great promise for large-scale application in water-splitting electrolyzers.

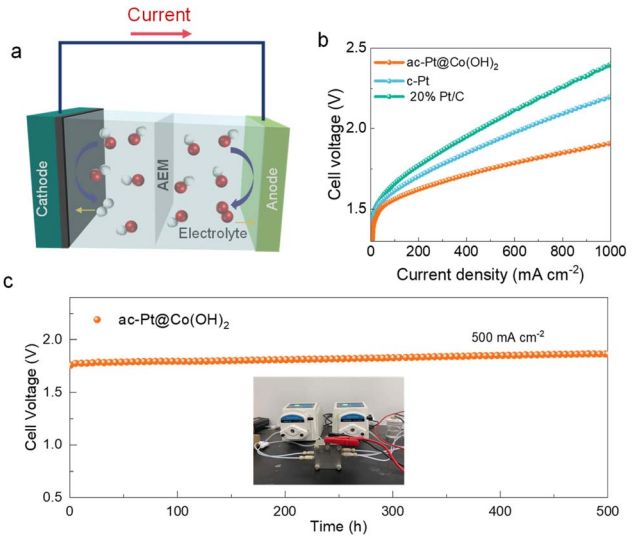


Fig. 5 (a) Schematic diagram of a membrane-electrode-assembly (MEA)-based AEMWE device. (b) Polarization curves of the AEMWE using ac-Pt@Co(OH)$_2$, c-Pt, and Pt/C. (c) Durability test of the ac-Pt@Co(OH)$_2$-based AEM electrolyser at a current density of 500 mA $cm^{-2}$. Insets show the photographs of the AEMWE device.

## 3 Conclusion

In summary, we have successfully synthesized an efficient c–a hetero-structured electrocatalyst composed of amorphous Co(OH)$_2$ and crystalline Pt for the alkaline HER. The abundant c–a interface along with strong Pt–Co interaction leads to optimized energy barriers for water dissociation and enhanced adsorption/desorption properties for the intermediates involved in the HER. The ac-Pt@Co(OH)$_2$ electrocatalyst displays excellent HER activity with an extremely low overpotential of 35 mV at 10 mA $cm^{-2}$ and a Tafel slope of 28.5 mV $dec^{-1}$, along with impressive continuous and cycling stability. The *in situ* characterization results reveal that the dynamic-cycling interfacial electronic interactions in c–a heterojunctions are responsible for water dissociation and improvement of reaction kinetics. Theoretical calculations reveal that amorphous Co(OH)$_2$ could improve water adsorption to supply abundant H species, and electronic rearrangement at the c–a interface downshifts the d-band center, thereby optimizing the desorption strength of *H for enhanced HER activity. This work highlights the potential of constructing catalysts with heterogeneous interfaces to optimize material electronic structures and boost intrinsic activity in various electrocatalytic reactions.

## Data availability

The data supporting the conclusions reached in this study have been included as part of the ESI.†

## Author contributions

J. P., H. S., P. T. and M. L. conceived the project. M. L. conducted the experiments, including catalyst synthesis, catalytic tests and data analysis. X. L. designed the *in situ* XAFS experiments. J. L. performed the *in situ* Raman measurements. Y. G. and F. L. performed the TEM tests. The manuscript was written by M. L., H. S and J. P. All authors discussed the results and commented on the paper.

## Conflicts of interest

The authors declare that they have no known competing financial interests or personal relationships that could have appeared to influence the work reported in this paper.

## Acknowledgements

The authors acknowledge support from the Postdoctoral Fellowship Program of CPSF under grant number GZB20240859, the National Natural Science Foundation of China (12405377 and 12205300), the China Postdoctoral Science Foundation (2024M763694), the Science and Technology Planning Project of Yunnan Province (202302AH360001), and the Natural Science Foundation of Hunan Province (2024JJ4027). The authors thank the staff at the 1W1B station at the Beijing Synchrotron Radiation Facility (BSRF) as well as the BL14W1 and BL20U beamlines at the Shanghai Synchrotron Radiation Facility (SSRF) for providing the beam time. The authors also acknowledge the staff at the infrared beamline (BL01B) of the National Synchrotron Radiation Laboratory for providing the beam time.

## Notes and references

1 G. Glenk and S. Reichelstein, Economics of converting renewable power to hydrogen, *Nat. Energy*, 2019, **4**, 216–222.
2 D. Strmcnik, M. Uchimura, C. Wang, R. Subbaraman, N. Danilovic, D. Van Der Vliet, A. P. Paulikas, V. R. Stamenkovic and N. M. Markovic, Improving the hydrogen oxidation reaction rate by promotion of hydroxyl adsorption, *Nat. Chem.*, 2013, **5**, 300–306.
3 X. Chen, X. T. Wang, J. B. Le, S. M. Li, X. Wang, Y. J. Zhang, P. Radjenovic, Y. Zhao, Y. H. Wang and X. M. Lin, Revealing the role of interfacial water and key intermediates at ruthenium surfaces in the alkaline hydrogen evolution reaction, *Nat. Commun.*, 2023, **14**, 5289.
4 L. Yang, H. Liu, Y. Li, L. Zhong, Z. Jin, X. Xu, D. Cao and Z. Chen, Customizing bonding affinity with multi-intermediates via interfacial electron capture to boost hydrogen evolution in alkaline water electrolysis, *Angew. Chem.*, 2025, **64**, e202414518.
5 S. Anantharaj, S. Kundu and S. Noda, Progress in nickel chalcogenide electrocatalyzed hydrogen evolution reaction, *J. Mater. Chem. A*, 2020, **8**, 4174–4192.
6 S. Anantharaj and S. Noda, Layered 2D $PtX_2$ (X= S, Se, Te) for the electrocatalytic HER in comparison with Mo/$WX_2$ and Pt/C: are we missing the bigger picture?, *Energy Environ. Sci.*, 2022, **15**, 1461–1478.
7 M. Smiljanic, S. Panic, M. Bele, F. Ruiz-Zepeda, L. Pavko, L. Gasparic, A. Kokalj, M. Gaberscek and N. Hodnik, Improving the HER activity and stability of Pt nanoparticles by titanium oxynitride support, *ACS Catal.*, 2022, **12**, 13021–13033.
8 W. Sheng, M. Myint, J. G. Chen and Y. Yan, Correlating the hydrogen evolution reaction activity in alkaline electrolytes with the hydrogen binding energy on monometallic surfaces, *Energy Environ. Sci.*, 2013, **6**, 1509–1512.
9 N. Danilovic, R. Subbaraman, D. Strmcnik, K. C. Chang, A. Paulikas, V. Stamenkovic and N. M. Markovic, Enhancing the alkaline hydrogen evolution reaction activity through the bifunctionality of $Ni(OH)_2$/metal catalysts, *Angew. Chem.*, 2012, **51**, 12495–12498.
10 Y. Liu, R. Duan, X. Li, L. Luo, J. Gong, G. Zhang, Y. Li and Z. Li, Unraveling the electronic effect of transition-metal dopants (M= Fe, Co, Ni, and Cu) and graphene substrate on platinum–transition metal dimers for hydrogen evolution reaction, *Inorg. Chem.*, 2022, **61**, 13210–13217.
11 J. Hu, C. Fang, X. Jiang, D. Zhang and Z. Cui, PtMn/PtCo alloy nanofascicles: robust electrocatalysts for electrocatalytic hydrogen evolution reaction under both acidic and alkaline conditions, *Inorg. Chem. Front.*, 2020, **7**, 4377–4386.
12 A. Jagminas, A. Naujokaitis, R. Žalnėravičius, V. Jasulaitiene and G. Valušis, Tuning the activity of nanoplatelet $MoS_2$-based catalyst for efficient hydrogen evolution via electrochemical decoration with Pt nanoparticles, *Appl. Surf. Sci.*, 2016, **385**, 56–62.
13 C. A. Zhou, K. Ma, Z. Zhuang, M. Ran, G. Shu, C. Wang, L. Song, L. Zheng, H. Yue and D. Wang, Tuning the local environment of Pt species at CNT@$MO_{2-x}$ (M= Sn and Ce) heterointerfaces for boosted alkaline hydrogen evolution, *J. Am. Chem. Soc.*, 2024, **146**, 21453–21465.
14 M. T. Koper and E. Bouwman, Electrochemical hydrogen production: bridging homogeneous and heterogeneous catalysis, *Angew. Chem.*, 2010, **49**, 3723–3725.
15 L. Hou, C. Li, H. Jang, M. G. Kim, J. Z. Jiang, J. Cho, S. Liu and X. Liu, Rationally designed Mo/Ru-based multi-site heterogeneous electrocatalyst for accelerated alkaline hydrogen evolution reaction, *Adv. Mater.*, 2024, **36**, 2410039.
16 Y. Zhang, Y. Lin, T. Duan and L. Song, Interfacial engineering of heterogeneous catalysts for electrocatalysis, *Mater. Today*, 2021, **48**, 115–134.
17 F. Tian, S. Geng, L. He, Y. Huang, A. Fauzi, W. Yang, Y. Liu and Y. Yu, Interface engineering: PSS-PPy wrapping amorphous Ni-Co-P for enhancing neutral-pH hydrogen evolution reaction performance, *Chem. Eng. J.*, 2021, **417**, 129232.

18 S. Zeng, D. Qu, H. Sun, Y. Chen, J. Wang, Y. Zheng, J. Pan, J. Cao and C. Li, Crystalline/amorphous interface engineering and d–sp orbital hybridization synergistically boosting the electrocatalytic performance of PdCu bimetallene toward formic acid-assisted overall water splitting, *ACS Appl. Mater. Interfaces*, 2024, **16**, 64797–64806.
19 S. Ju, Y. Liu, M. Pei, Y. Shuai, Z. Zhai, W. Yan, Y.-J. Wang and J. Zhang, Amorphization-induced abundant coordinatively unsaturated Ni active sites in $NiCo(OH)_2$ for boosting catalytic OER and HER activities at high current densities for water-electrolysis, *J. Colloid Interface Sci.*, 2024, **653**, 1704–1714.
20 Y. Zhang, F. Gao, D. Wang, Z. Li, X. Wang, C. Wang, K. Zhang and Y. Du, Amorphous/crystalline heterostructure transition-metal-based catalysts for high-performance water splitting, *Coord. Chem. Rev.*, 2023, **475**, 214916.
21 L. Liang, H. Jin, H. Zhou, B. Liu, C. Hu, D. Chen, Z. Wang, Z. Hu, Y. Zhao and H.-W. Li, Cobalt single atom site isolated Pt nanoparticles for efficient ORR and HER in acid media, *Nano Energy*, 2021, **88**, 106221.
22 N. Guo, H. Xue, J. Sun, T. Song, H. Dong, Z. Zhao, J. Zhang, Q. Wang and L. Wu, In-situ electrochemical self-reconstruction of permeable Ni $(OH)_2$/Pt hybrid for accelerating alkaline hydrogen evolution, *Next Mater.*, 2024, **3**, 100109.
23 Z. Zhao, H. Liu, W. Gao, W. Xue, Z. Liu, J. Huang, X. Pan and Y. Huang, Surface-engineered PtNi-O nanostructure with record-high performance for electrocatalytic hydrogen evolution reaction, *J. Am. Chem. Soc.*, 2018, **140**, 9046–9050.
24 Y. Gu, Y. Wang, J. Shi, M. Yang, Y. Rui, W. An and Y. Men, Well-dispersed Pt nanodots interfaced with $Ni(OH)_2$ on anodized nickel foam for efficient hydrogen evolution reaction, *Int. J. Hydrogen Energy*, 2020, **45**, 27067–27077.
25 Q. Liu, Z. Yan, J. Gao, E. Wang and G. Sun, Optimizing platinum location on nickel hydroxide nanosheets to accelerate the hydrogen evolution reaction, *ACS Appl. Mater. Interfaces*, 2020, **12**, 24683–24692.
26 S. Lu and Z. Zhuang, Investigating the influences of the adsorbed species on catalytic activity for hydrogen oxidation reaction in alkaline electrolyte, *J. Am. Chem. Soc.*, 2017, **139**, 5156–5163.
27 S. Xin, Y. Tang, B. Jia, Z. Zhang, C. Li, R. Bao, C. Li, J. Yi, J. Wang and T. Ma, Coupling adsorbed evolution and lattice oxygen mechanism in Fe-$Co(OH)_2/Fe_2O_3$ heterostructure for enhanced electrochemical water oxidation, *Adv. Funct. Mater.*, 2023, **33**, 2305243.
28 C. Wan, Z. Zhang, J. Dong, M. Xu, H. Pu, D. Baumann, Z. Lin, S. Wang, J. Huang and A. H. Shah, Amorphous nickel hydroxide shell tailors local chemical environment on platinum surface for alkaline hydrogen evolution reaction, *Nat. Mater.*, 2023, **22**, 1022–1029.
29 L. Gao, C. Guo, X. Sun, X. Sun, H. Yang, J. Xie, X. Ma, M. Zhao, X. Zhu and Q. Wei, $CoFeO_x$ $(OH)_y/CoO_x(OH)_y$ core/shell structure with amorphous interface as an advanced catalyst for electrocatalytic water splitting, *Electrochim. Acta*, 2020, **341**, 136038.
30 X. Zhang, S. Zhu, L. Xia, C. Si, F. Qu and F. Qu, $Ni(OH)_2$–$Fe_2P$ hybrid nanoarray for alkaline hydrogen evolution reaction with superior activity, *Chem. Commun.*, 2018, **54**, 1201–1204.
31 Y. Z. Su, K. Xiao, N. Li, Z. Q. Liu and S. Z. Qiao, Amorphous $Ni(OH)_2$ @ three-dimensional Ni core–shell nanostructures for high capacitance pseudocapacitors and asymmetric supercapacitors, *J. Mater. Chem. A*, 2014, **2**, 13845–13853.
32 H. Sun, M. Chen, B. Xiao, T. Zhou, M. Humayun, L. Li, Q. Lu, T. He, J. Zhang and M. Bououdina, Interface engineering induced electron redistribution at PtNs/NiTe-Ns interfaces for promoting pH-universal and chloride-tolerant hydrogen evolution reaction, *Small*, 2023, **19**, 2303974.
33 M. Liu, S. Bo, J. Zhang, Q. Liu, J. Pan and H. Su, Tracking the role of compressive strain in bowl-Like Co-MOFs structural evolution in water oxidation reaction, *Appl. Catal., B*, 2024, **354**, 124114.
34 M. Liu, X. Chen, S. Li, C. Ni, Y. Chen and H. Su, Dynamic-cycling zinc sites promote ruthenium oxide for sub-ampere electrochemical water oxidation, *Nano Lett.*, 2024, **24**, 16055–16063.
35 G. Wu, X. Han, J. Cai, P. Yin, P. Cui, X. Zheng, H. Li, C. Chen, G. Wang and X. Hong, In-plane strain engineering in ultrathin noble metal nanosheets boosts the intrinsic electrocatalytic hydrogen evolution activity, *Nat. Commun.*, 2022, **13**, 4200.
36 H. Wu, X. Zuo, S. P. Wang, J. W. Yin, Y. N. Zhang and J. Chen, Theoretical and experimental design of Pt-Co $(OH)_2$ electrocatalyst for efficient HER performance in alkaline solution, *Prog. Nat. Sci.:Mater. Int.*, 2019, **29**, 356–361.
37 Y. Hong, C. H. Choi and S. I. Choi, Catalytic surface specificity of Ni $(OH)_2$-decorated Pt nanocubes for the hydrogen evolution reaction in an alkaline electrolyte, *ChemSusChem*, 2019, **12**, 4021–4028.
38 Z. Jiang, J. Ren, Y. Li, X. Zhang, P. Zhang, J. Huang, C. Du and J. Chen, Low-cost high-performance hydrogen evolution electrocatalysts based on Pt-CoP polyhedra with low Pt loading in both alkaline and neutral media, *Dalton Trans.*, 2019, **48**, 8920–8930.
39 Y. Shi, Z. R. Ma, Y. Y. Xiao, Y. C. Yin, W. M. Huang, Z. C. Huang, Y. Z. Zheng, F. Y. Mu, R. Huang and G. Y. Shi, Electronic metal–support interaction modulates single-atom platinum catalysis for hydrogen evolution reaction, *Nat. Commun.*, 2021, **12**, 3021.
40 A. Pei, R. Xie, Y. Zhang, Y. Feng, W. Wang, S. Zhang, Z. Huang, L. Zhu, G. Chai and Z. Yang, Effective electronic tuning of Pt single atoms via heterogeneous atomic coordination of (Co, Ni)$(OH)_2$ for efficient hydrogen evolution, *Energy Environ. Sci.*, 2023, **16**, 1035–1048.
41 Z. Xing, C. Han, D. Wang, Q. Li and X. Yang, Ultrafine Pt nanoparticle-decorated Co $(OH)_2$ nanosheet arrays with enhanced catalytic activity toward hydrogen evolution, *ACS Catal.*, 2017, **7**, 7131–7135.
42 W. Xu, J. Chang, Y. Cheng, H. Liu, J. Li, Y. Ai, Z. Hu, X. Zhang, Y. Wang and Q. Liang, A multi-step induced strategy to fabricate core-shell Pt-Ni alloy as symmetric electrocatalysts for overall water splitting, *Nano Res.*, 2022, **15**, 965–971.

43 A. Fan, P. Zheng, C. Qin, X. Zhang, X. Dai, D. Ren, X. Fang, C. Luan and J. Yang, Few-layer $MoS_2$ and Pt nanoparticles Co-anchored on MWCNTs for efficient hydrogen evolution over a wide pH range, *Electrochim. Acta*, 2020, **358**, 136927.

44 L. Xie, X. Ren, Q. Liu, G. Cui, R. Ge, A. M. Asiri, X. Sun, Q. Zhang and L. Chen, A Ni $(OH)_2$–$PtO_2$ hybrid nanosheet array with ultralow Pt loading toward efficient and durable alkaline hydrogen evolution, *J. Mater. Chem. A*, 2018, **6**, 1967–1970.

45 Z. Cao, Q. Chen, J. Zhang, H. Li, Y. Jiang, S. Shen, G. Fu, B.-a. Lu, Z. Xie and L. Zheng, Platinum-nickel alloy excavated nano-multipods with hexagonal close-packed structure and superior activity towards hydrogen evolution reaction, *Nat. Commun.*, 2017, **8**, 15131.

46 J. Fan, K. Qi, L. Zhang, H. Zhang, S. Yu and X. Cui, Engineering Pt/Pd interfacial electronic structures for highly efficient hydrogen evolution and alcohol oxidation, *ACS Appl. Mater. Interfaces*, 2017, **9**, 18008–18014.

47 P. Kuang, Y. Wang, B. Zhu, F. Xia, C. W. Tung, J. Wu, H. M. Chen and J. Yu, Pt single atoms supported on N-doped mesoporous hollow carbon spheres with enhanced electrocatalytic $H_2$-evolution activity, *Adv. Mater.*, 2021, **33**, 2008599.

48 L. Zeng, Z. Zhao, F. Lv, Z. Xia, S.-Y. Lu, J. Li, K. Sun, K. Wang, Y. Sun and Q. Huang, Anti-dissolution Pt single site with $Pt(OH)(O_3)$/Co(P) coordination for efficient alkaline water splitting electrolyzer, *Nat. Commun.*, 2022, **13**, 3822.

49 K. Jiang, B. Liu, M. Luo, S. Ning, M. Peng, Y. Zhao, Y. R. Lu, T. S. Chan, F. M. de Groot and Y. Tan, Single platinum atoms embedded in nanoporous cobalt selenide as electrocatalyst for accelerating hydrogen evolution reaction, *Nat. Commun.*, 2019, **10**, 1743.

50 M. Liu, J. Zhang, H. Su, Y. Jiang, W. Zhou, C. Yang, S. Bo, J. Pan and Q. Liu, In situ modulating coordination fields of single-atom cobalt catalyst for enhanced oxygen reduction reaction, *Nat. Commun.*, 2024, **15**, 1675.

51 M. Liu, X. Zhong, X. Chen, D. Wu, C. Yang, S. Li, C. Ni, Y. Chen, Q. Liu and H. Su, Unraveling compressive strain and oxygen vacancy effect of iridium oxide for proton-exchange membrane water electrolyzers, *Adv. Mater.*, 2025, 2501179.

52 L. Cao, Q. Luo, W. Liu, Y. Lin, X. Liu, Y. Cao, W. Zhang, Y. Wu, J. Yang and T. Yao, Identification of single-atom active sites in carbon-based cobalt catalysts during electrocatalytic hydrogen evolution, *Nat. Catal.*, 2019, **2**, 134–141.

53 H. Su, C. Yang, M. Liu, X. Zhang, W. Zhou, Y. Zhang, K. Zheng, S. Lian and Q. Liu, Tensile straining of iridium sites in manganese oxides for proton-exchange membrane water electrolysers, *Nat. Commun.*, 2024, **15**, 95.

54 M. Zhong, M. Xu, S. Ren, W. Li, C. Wang, M. Gao and X. Lu, Modulating the electronic structure of $Ni(OH)_2$ by coupling with low-content Pt for boosting the urea oxidation reaction enables significantly promoted energy-saving hydrogen production, *Energy Environ. Sci.*, 2024, **17**, 1984–1996.

55 L. Cao, F. A. Soto, D. Li, T. Deng, E. Hu, X. Lu, D. A. Cullen, N. Eidson, X. Q. Yang and K. He, Pd-Ru pair on Pt surface for promoting hydrogen oxidation and evolution in alkaline media, *Nat. Commun.*, 2024, **15**, 7245.

56 Y. Wu, M. Chen, D. Liu, H. Sun, T. Zhou, G. Na, G. Qiu, D. Li, Y. Chen and J. Zhao, Modulating the synergy of Pt single atoms and quantum dots on NiFe LDH for efficient and robust hydrogen evolution, *J. Mater. Sci. Technol.*, 2025, **215**, 111–120.

57 L. F. Shen, B. A. Lu, Y. Y. Li, J. Liu, Z. C. Huang, H. Peng, J. J. Ye, X. M. Qu, J. M. Zhang, G. Li, W. B. Cai, Y. X. Jiang and S. G. Sun, Interfacial structure of water as a new descriptor of the hydrogen evolution reaction, *Angew. Chem.*, 2020, **59**, 22397–22402.

58 S. Shen, Z. Wang, Z. Lin, K. Song, Q. Zhang, F. Meng, L. Gu and W. Zhong, Crystalline-amorphous interfaces coupling of $CoSe_2$/CoP with optimized d-band center and boosted electrocatalytic hydrogen evolution, *Adv. Mater.*, 2022, **34**, 2110631.

59 D. Wang, W. Liu, H. Wang, S. Lu, Y. Li, S. Guo and Y. Xiang, Dual modulation of hydroxyl action on ruthenium surface by single-atom supports for alkaline $H_2$ evolution, *Adv. Funct. Mater.*, 2024, 2417976.